

Periodicity hubs and spirals in an electrochemical oscillator

Melke A. Nascimento · Hamilton Varela ·
Jason A. C. Gallas

Received: 27 December 2014 / Revised: 28 January 2015 / Accepted: 17 February 2015 / Published online: 5 March 2015
© Springer-Verlag Berlin Heidelberg 2015

Abstract The control parameter space of lasers, electronic circuits, and biological oscillators was recently discovered to be riddled with remarkable points, called periodicity hubs, responsible for a wide-ranging self-organization of the systems. Although displaying features which resemble the organization seen in chemical models, periodicity hubs have not been detected in such models thus far. Here, we report numerical evidence that periodicity hubs and the infinite spirals of stable oscillations issuing from them exist profusely in an electrochemical

oscillator model. For selected parameter ranges, we observe sequences of *nonchaos-mediated* mixed-mode oscillations. Chemical hubs open the possibility of studying experimentally the complex self-organization of stable oscillations and complicated phenomena of current interest. We report high-resolution stability diagrams providing reference charts to guide experimental work as well as stringent tests for the validity of the electrochemical oscillator model used.

Keywords Self-organization in electrochemistry · Electrochemical oscillators · Nonchaos-mediated mixed-mode oscillations · Chemical hubs · Phase diagrams

M. A. Nascimento · H. Varela
Institute of Chemistry of São Carlos, University of São Paulo,
PO Box 780, 13560-970 São Carlos, SP, Brazil

H. Varela
Ertl Center for Electrochemistry and Catalysis,
GIST, Cheomdan-gwagiro 261, Buk-gu,
Gwangju 500-712, South Korea

J. A. C. Gallas (✉)
Departamento de Física, Universidade Federal da Paraíba,
58039-970 João Pessoa, Brazil
e-mail: jason.gallas@gmail.com

J. A. C. Gallas
Instituto de Altos Estudos da Paraíba, Rua Infante Dom Henrique
100-1801, 58051-150 João Pessoa, Brazil

J. A. C. Gallas
Institute for Multiscale Simulation, Friedrich-Alexander
Universität Erlangen-Nürnberg, 91052 Erlangen,
Germany

J. A. C. Gallas
Max Planck Institute for the Physics of Complex Systems,
Nöthnitzer Straße 38, 01187 Dresden, Germany

Introduction

Complex temporal dynamics including multistability, excitability, quasiperiodicity, self-pulsing, bursting, and deterministic chaos, as well as spatiotemporal pattern formation occur in many chemical, physical, and biological systems [1–6]. Phase diagrams describing the intricacies of the self-organization of oscillatory motions with high periods and chaotic phases comprise a subject that has come to the fore over the last few years [7–30]. An up-to-date and encompassing treatment of self-organization in electrochemical systems can be found in [3].

Until recently, phase diagrams were regarded as a highly difficult subject, accessible only to those willing to perform massive computations over wide ranges in the space of control parameters. When dealing with nonlinear dynamical systems, phase diagrams traditionally display just a few curves intended mainly to delimit the boundaries between

steady-state solutions and boundaries emerging immediately after them, mainly after Hopf bifurcations. Furthermore, the overwhelming majority of the existing phase diagrams amount to applications of a specific *continuation software* that focus on *unstable mathematical phenomena*, i.e., on something that cannot be readily measured in laboratory experiments. Although mathematically interesting, in general, such diagrams of unstable phenomena cannot be compared with observed or measured ones. Thus, three decades of extensive studies of deterministic chaos notwithstanding, it is only more recently that phase diagrams detailing the structure of *stable* (measurable) motions of high-periodicity and chaos started to emerge. And they have been proving an inexhaustible source of unanticipated and interesting facts [7–30].

In this paper, we focus on a remarkable set of points, called *periodicity hubs*, discovered abundantly in the control parameter space of lasers of several types, in electronic circuits, in biological oscillators, and in other nonlinear oscillators. Such hubs are the common focal points where a doubly infinite set of spiral phases, regular and chaotic, characterized by stable oscillations of specific waveforms accumulate [8, 10, 27, 29]. In such points, which exist abundantly spread in parameter space, one may commute from one spiral to any of the double infinite other spirals, of regularity or of chaos. The spirals of stability stretch over wide ranges in parameter space and, accordingly, induce a characteristic global organization of the control parameter space.

The purpose of this work is to further develop our recent study [19] and report results of extended numerical simulations that provide evidence of the presence of periodicity hubs and spirals in a minimal model of a generic model of an electrochemical oscillator. The model under consideration is a prototype of a paradigmatic class of oscillators that includes most fuel cell anodic reactions [31–39], so that the results presented here should also assist the quest for the experimental detection of such novel phenomena in these systems.

The electrochemical oscillator model

The model investigated here was introduced by Krischer [40] based on previous propositions [41, 42], and represents a prototype for the HN-NDR class of electrochemical oscillators whose main feature is the presence of a partially hidden (H) negative differential resistance (NDR) in an *N*-shaped current-potential curve [43, 44].

Denoting by φ the double layer potential, by c the concentration of electroactive species, and by θ the surface coverage of an inhibiting species that blocks the faradaic

reaction, the model consists of a dissipative flow defined by the following nonlinear differential equations:

$$\varepsilon \frac{d\varphi}{dt} = -I_F + \frac{U - \varphi}{\rho}, \quad (1)$$

$$\frac{d\theta}{dt} = \theta_0(\varphi) - \theta, \quad (2)$$

$$\mu \frac{dc}{dt} = -k(\varphi)(1 - \theta)c + 1 - c, \quad (3)$$

In the equations above, the parameter ε defines the time scale for the evolution of the electrode potential, μ accounts for the time-scale of the temporal evolution of c , U is the applied voltage, and ρ is the total resistance. The left-hand side term in Eq. 1 is the capacitive current, whereas the right-hand side terms are the faradaic current, $I_F = k(\varphi)(1 - \theta)c$, and the total current. The functions $k(\varphi)$, representing the potential-dependent reaction rate constant, and θ_0 , representing the equilibrium surface coverage of a poison species, are given, respectively, by

$$k(\varphi) = 0.00002\varphi^3 - 0.0094\varphi^2 + 1.12\varphi, \quad (4)$$

$$\theta_0(\varphi) = \left[1 + \exp\left(\frac{\varphi - \varphi_0}{b}\right) \right]^{-1}. \quad (5)$$

Simulations were carried out for $b = 7.1204$, $\varphi_0 = 124.6$, $\mu = 50$, and ε was varied from 0.001 to 0.012 (in contrast to $\varepsilon = 0.001$ used in our previous work [19]). As may be recognized from Eqs. 1 and 3 above, the specific values of ε and μ are important for controlling the relative time scales of the chemical dynamics. The parameter ε accounts for the time-scale of the changes in the double layer potential and is proportional to the electrode capacitance. As far as experiments are concerned, the capacitance can be varied to a considerable extent by changing the electrode roughness, for instance.

Computational details

Our results are displayed in two complementary types of phase diagrams, namely the standard diagrams based on Lyapunov exponents [1, 2], and the much richer *isospine diagrams* [10, 45–47].

We computed the Lyapunov exponents by solving (1–3) numerically with a standard fourth-order Runge-Kutta algorithm with fixed-step, $h = 0.001$, over a high-resolution mesh consisting of $1200 \times 1200 = 1.44 \times 10^6$ equally spaced points. For each mesh point, we computed the three exponents by starting numerical integrations always from the same fixed arbitrarily chosen initial condition: $(x, y, z) = (150, 0.5, 0.06)$. The first 2×10^5 time-steps were discarded as transient time needed to reach the final attractor. The subsequent 4×10^6 iterations

were then used to compute the Lyapunov spectrum of the oscillator.

The isospike diagrams were obtained after computing Lyapunov exponents, by recording up to 800 extrema (local maxima and minima) of the three time series of the system, together with the instant of time that they occurred and recording repetitions of the maxima. A palette of 17 colors was used to represent “modulo 17” the number of peaks (local maxima) in one period of the oscillations, i.e., by recycling the 17 colors according to the number of spikes contained in one period. Black was used to represent chaotic oscillations, namely lack of numerically detectable periodicity.

The investigation of each parameter point demands the additional investigation of a basin of attraction in phase-space, a task involving an additional square grid, but of variables (instead of parameters). For this reason, the computation of high-resolution stability diagrams for several millions of points is a quite demanding task. We performed such task with the help of 1536 high-performance processors of a SGI Altix cluster with a theoretical peak performance of 16 Tflops.

Results

Figure 1 shows high-resolution stability diagrams computed for $\varepsilon = 0.005$. Individual panels display the analysis of the dynamics for 1200×1200 parameter points, i.e., for well over a million points per diagram. Figure 1a–d shows a sequence of four Lyapunov phase diagrams computed as described in the previous Section. Figure 1a shows a very large portion of the $U \times \rho$ control parameter space. The wide white region represents non-oscillating solutions with non-zero amplitude while the gray region is characterized by self-induced oscillations. Accordingly, the boundary delimiting these two phases is a line characterized by Hopf bifurcations. As indicated by the color table, the largest part of gray phase contains periodic oscillations, characterized by negative Lyapunov exponents. However, when compared to previously published data [19] obtained for smaller ε (i.e., for $\varepsilon = 0.001$), the first observation to be pointed out consists of the relative size of the chaotic region contained in Fig. 1. The effect of increasing ε results in a considerable concentration of the regions of positive Lyapunov. Nevertheless, the existing region of chaotic dynamics remains localized in a relatively similar region in the $U \times \rho$ plane than found for smaller ε . In addition, the structure of periodic gray lines qualitatively follows our previous study, despite the fact that, in the present case, these lines are not intercalated with chaotic ones. In other words, while for $\varepsilon = 0.001$ there is a standard cascade of mixed-mode oscillations, for $\varepsilon = 0.005$ we find

nonchaos-mediated sequences of mixed-mode oscillations similar to the one discovered very recently in an enzyme reaction system [8].

A large number of details concerning the organization of families of periodic oscillations and chaos are given in the Fig. 1b–d. Overall, at this magnification, an intricate dynamics where cascades of somewhat rounded structures prevail embedded in chaotic region is observed, as better evidenced by the dark arcs in Fig. 1d. The alternation between chaos and periodic domains depicted in this figure resembles somewhat the results found in another chemical flow [28]. Finally, it is also remarkable that the borders separating chaotic and periodic domains are rather smooth when compared to the ones found for $\varepsilon = 0.001$ (see [19]).

The three panels in the bottom row of Fig. 1 show a magnified view of the region contained in the white box in Fig. 1c. They illustrate the aforementioned isospike diagrams [10, 45–47]. As indicated by the color table underneath, the isospike diagrams in Fig. 1e–g display the distribution of spikes contained inside one period of the periodic oscillations as counted in the three variables of the model, φ , θ , c , respectively. From the isospike diagrams, one sees that the boundaries of the stability domains do not depend of the variable used to count the spikes. The diagrams also show that the number of spikes change in different regions of the control space, sensitively depending on the variable used to count the spikes. It is important to emphasize that, while the Lyapunov diagram contained in the white box of Fig. 1c only discriminates between chaos and periodicity, in addition to this information, the three isospike diagrams reveal the precise location where the number of spikes change according to each dynamical variable of the problem.

Figure 2 shows the fine structure observed within the chaotic domains presented in smaller blue box in Fig. 1c. The shrimp-like periodic regions seen in the figure were already detected and described in our previous work [19, 20]. Here, however, the novelty is that they emerge organized in a quite distinctive way, forming spirals around certain centers, called *periodicity hubs*, similarly as first predicted for an electronic circuit involving diodes [27, 29], and subsequently observed experimentally in a Duffing-like autonomous oscillator [14].

Figure 2a contains two pairs of circles centered on the successive shrimps of the spiralling around the common periodicity hub. The electrochemical oscillator under consideration is strongly dissipative, a fact that implies strong compression of the arms of the spirals making them difficult to visualize with the help of ad hoc zooming in the control space, as illustrated by the additional circles in Fig. 2b–d. The spiralling shown in Fig. 2 accumulates at a focal point located roughly along the line segment joining the center

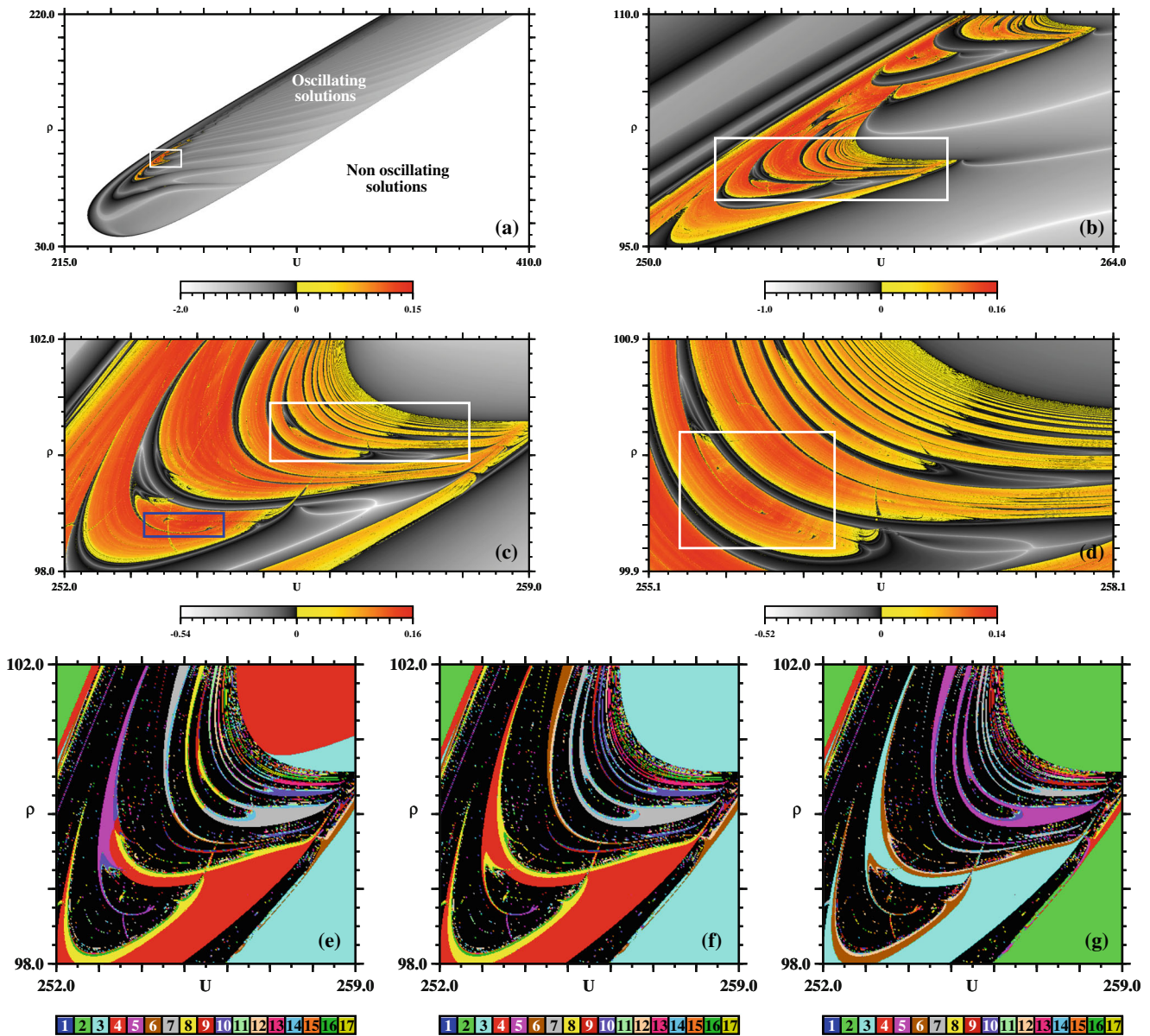


Fig. 1 Panels **a–d**: Four Lyapunov stability diagrams showing successive magnifications as indicated by the white boxes. *Gray shadings* indicate periodic oscillations (*negative exponents*), *colors* denote chaos (*positive exponents*). The *large white region* in **(a)** marks non-oscillating, non-zero solutions. Panel **d** illustrates typical accumulations observed in the control plane of the electrochemical oscillator. Such accumulations contain infinite cascades of periodicity hubs and spirals which accumulate towards the upper right corner (see Fig. 2).

Panels **e–g** in the bottom row are *isospike diagrams* (see text) for the variables φ , θ , and c , respectively. They are magnifications of the white box in **(e)**, and show that the number of spikes in one period of the periodic oscillations depends of the variable used to count them. The smaller box in **(c)** is magnified in Fig. 2a. Here, $\varepsilon = 0.005$ and $\mu = 50$. Individual panels display the analysis of $1200 \times 1200 = 1.44 \times 10^6$ parameter points

of the pair of smaller circles in Fig. 2d. By the arguments presented by Vitolo et al. [21], we know that such remarkable organizing focal centers form infinite hierarchies of points which exist inside every one of the chaotic phases delimited by the rounded dark segments easily discernible in Fig. 1d and accumulating towards the rightmost upper corner of the figure. Every such point is an accumulation point

of an infinite hierarchy of nested spirals of periodicity and chaos.

It is interesting to mention that Sparrow and Glendinning [24] and Gaspard, Kapral, and Nicolis [25] had already described some characteristics of the formation of spirals. However, apart from other details, these works do not indicate the exact structure of the complex shrimps forming

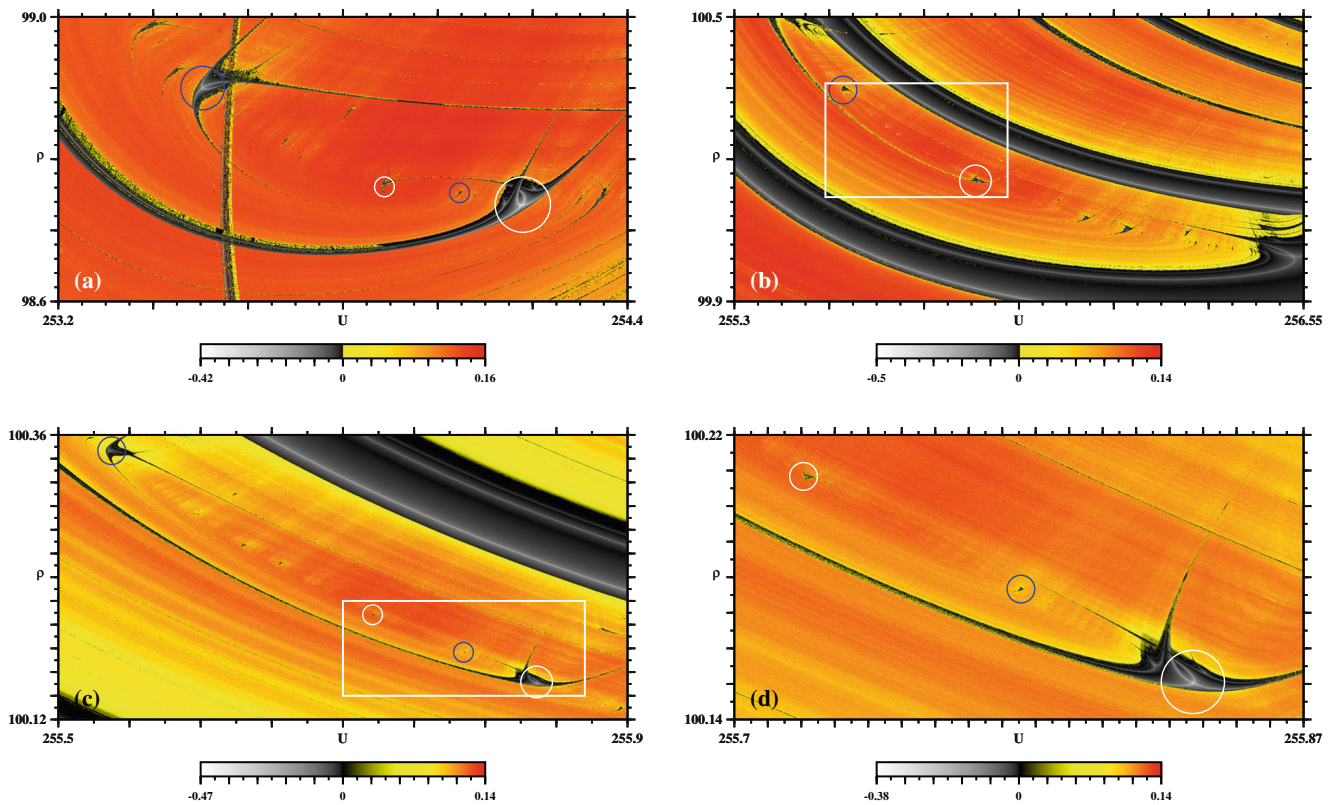


Fig. 2 Details of the anti-clockwise spiralling around the periodicity hubs. The pair of circles with similar colors mark the location of two successive *shrims* along two of the infinite spiral stability domains. The strong compression renders invisible the full spirals

in the scales of these panels but are visible when magnified. Negative exponents refer to phases characterized by periodic oscillations, whereas positive exponents denote chaotic phases. Individual panels display the analysis of $1200 \times 1200 = 1.44 \times 10^6$ parameter points

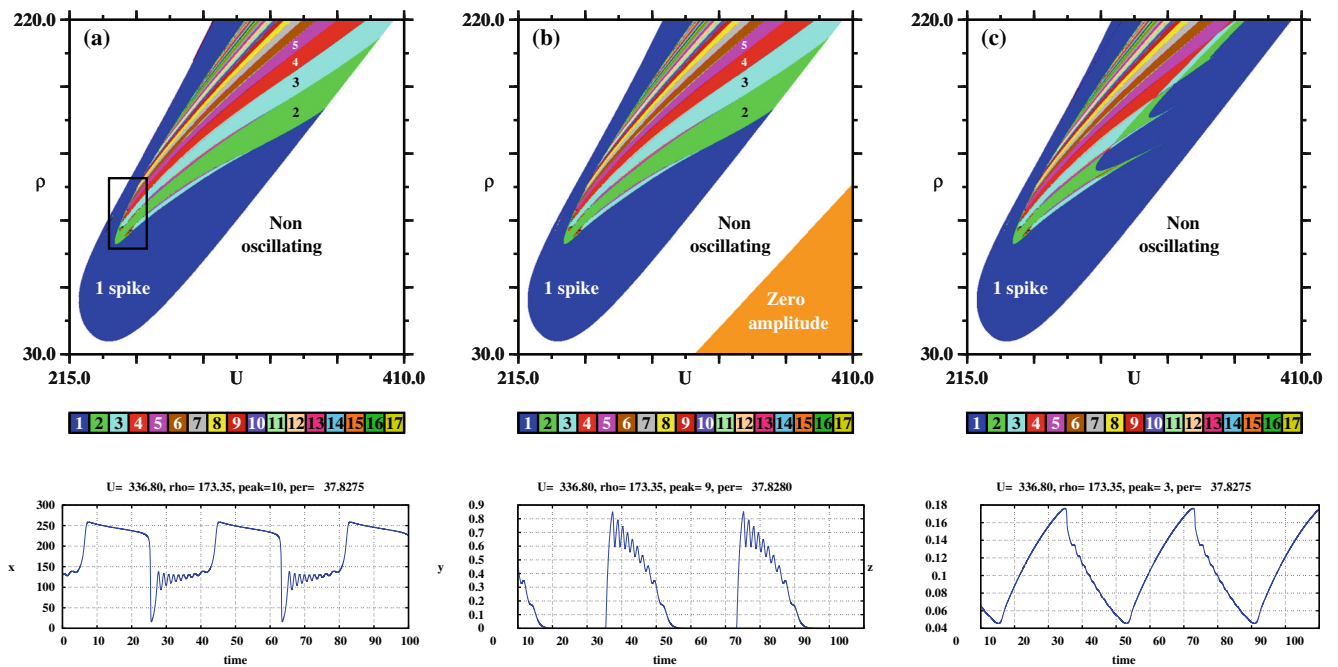
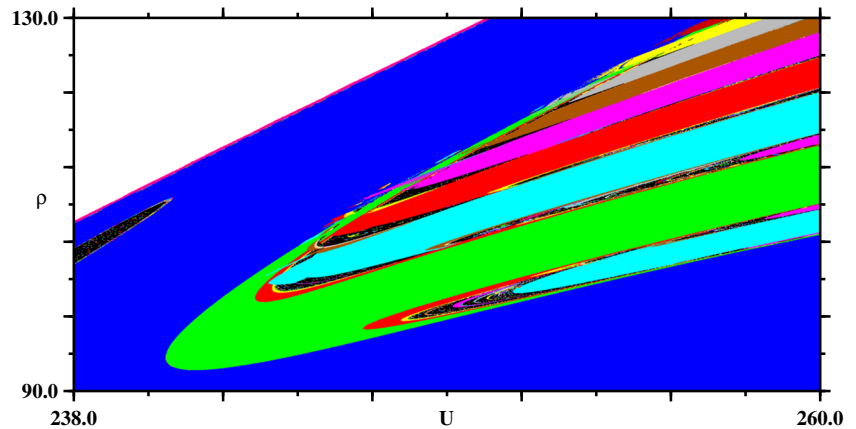


Fig. 3 Qualitative differences observed in the stability phases when counting spikes for three dynamical variables. **a** Counting spikes of φ , **b** spikes of θ , and **c** spikes of c . The three temporal evolutions in the

bottom row illustrate that c has less pronounced spikes than the other two variables. Here, $\varepsilon = 0.001$. The box in panel **a** is shown enlarged in Fig. 4. “Zero amplitude” means $\theta = 0$ in this region

Fig. 4 Magnification of the box in Fig. 3a revealing that, in suitable parameter ranges, the periodic oscillations of the electrochemical oscillator unfold according to a Stern-Brocot tree [45–50]. See text. Here $\varepsilon = 0.001$



the spirals, they contain no mention of the chaotic phases necessarily present in the spiralling, and, more importantly, they do not describe neither the infinite nesting of hubs and spirals nor the accumulation of spirals at the periodicity hubs. Earlier works described spirals as a necessary consequence of the homoclinic behavior for parameters obeying Shilnikov conditions, namely for parameters that can be associated with a fixed point of a saddle-focus type characterized by eigenvalues $(\lambda, \gamma \pm i\omega)$ and obeying the inequality $|\gamma/\lambda| < 1$. But it is known that this Shilnikov condition is not necessary to produce hubs and spirals. For instance, Freire and Gallas [26] showed that a semiconductor laser with optoelectronic feedback displays hubs and spirals independently of the Shilnikov condition. Details of the specific mechanisms underlying spirals generated by Shilnikov's condition have been discussed in

two recent papers, by Vitolo and co-workers [21] and by Shilnikov and co-workers [22, 23]. Using Rössler's oscillator as a working-example, both works explain that the structural properties of hubs and spirals originate from fold- and cusp-shaped bifurcation curves of saddle-node periodic orbits.

Figure 3 shows the control parameter space structural organization in terms of the spikes contained in one period of the oscillations, counted for the three variables of the electrochemical oscillator. As indicated, the large blue region corresponds to oscillations containing a single spike per period. The numbers in panels (a) and (b) indicate the number of spikes of the regions containing them. The simultaneous increase of ρ and U produces a regular addition of spikes as the one typically associated with mixed-mode oscillation in electrochemical systems [7, 51]. However, in

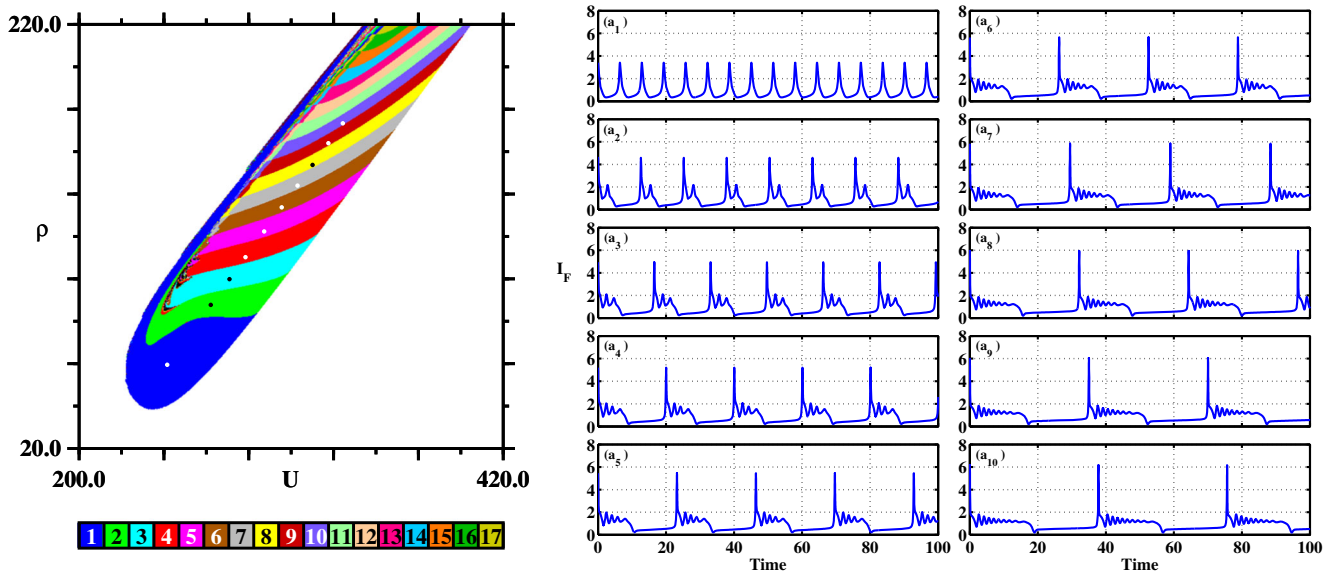


Fig. 5 Typical temporal evolutions a_ℓ , displaying ℓ spikes in one period of φ , the double layer potential, recorded when simultaneously tuning U and ρ across the stripes of the isospike diagram on the left

panel, at the ten points along the line $\rho = -247.65 + 1.25 U$ with coordinates given in Table 1. Here, $\varepsilon = 0.005$

Table 1 Coordinates of the ten points in Fig. 5 and the period of the oscillations of φ , the double layer potential

U	ρ	Spikes	Period
245.70	59.47	1	6.44
268.30	87.72	2	12.61
278.00	99.85	3	16.55
286.30	110.22	4	20.04
296.00	122.35	5	23.21
305.10	133.72	6	26.28
313.30	143.97	7	29.26
321.10	153.72	8	32.17
329.30	163.97	9	35.02
336.80	173.35	10	37.82

contrast to the standard unfolding of mixed-mode oscillations, where a chaotic phase is always observed before an increase of the number of spikes, here we find nonchaos-mediated transitions, similar to the transitions observed recently in a ten-dimensional model of an enzyme reaction [8]. With hindsight, the same unfolding can be recognized in the control space of a CO₂ laser with feedback [9].

While Fig. 3a, b look relatively similar, Fig. 3c looks different, with the stripes of periodic oscillations being

interrupted irregularly. To understand this difference, the last row of Fig. 3 shows the temporal evolution of φ , θ , and c . From them, one recognizes that the spikes of c are by far less pronounced than the spikes in the other two variables. When parameters change, these spikes tend to disappear, resulting in the aforementioned abrupt interruptions.

Is there a systematic way of classifying the regular self-organization of oscillations displayed in Fig. 3? To this end, Fig. 4 shows a magnification of the parameter region contained in the black box in Fig. 3a. Recently, it was shown that the most general possible organization of mixed-mode oscillations involves not the asymmetric Farey tree, as usually presumed but, instead, the more general and symmetric Stern-Brocot tree [45–50]. Figure 4 shows that the oscillations of the electrochemical oscillator emerge also organized following in a Stern-Brocot tree, at least for the parameters that we are considering. The Stern-Brocot is robust around $\varepsilon = 0.001$ but, of course, does not remain valid for arbitrarily changes. In particular, it is no longer valid for $\varepsilon = 0.005$ (see Fig. 5) where the organization is rather different from either the Farey or the Stern-Brocot organization.

The leftmost panel in Fig. 5 shows an isospike diagram obtained by counting the spikes of the periodic oscillations of φ , the double layer potential. This diagram contains a

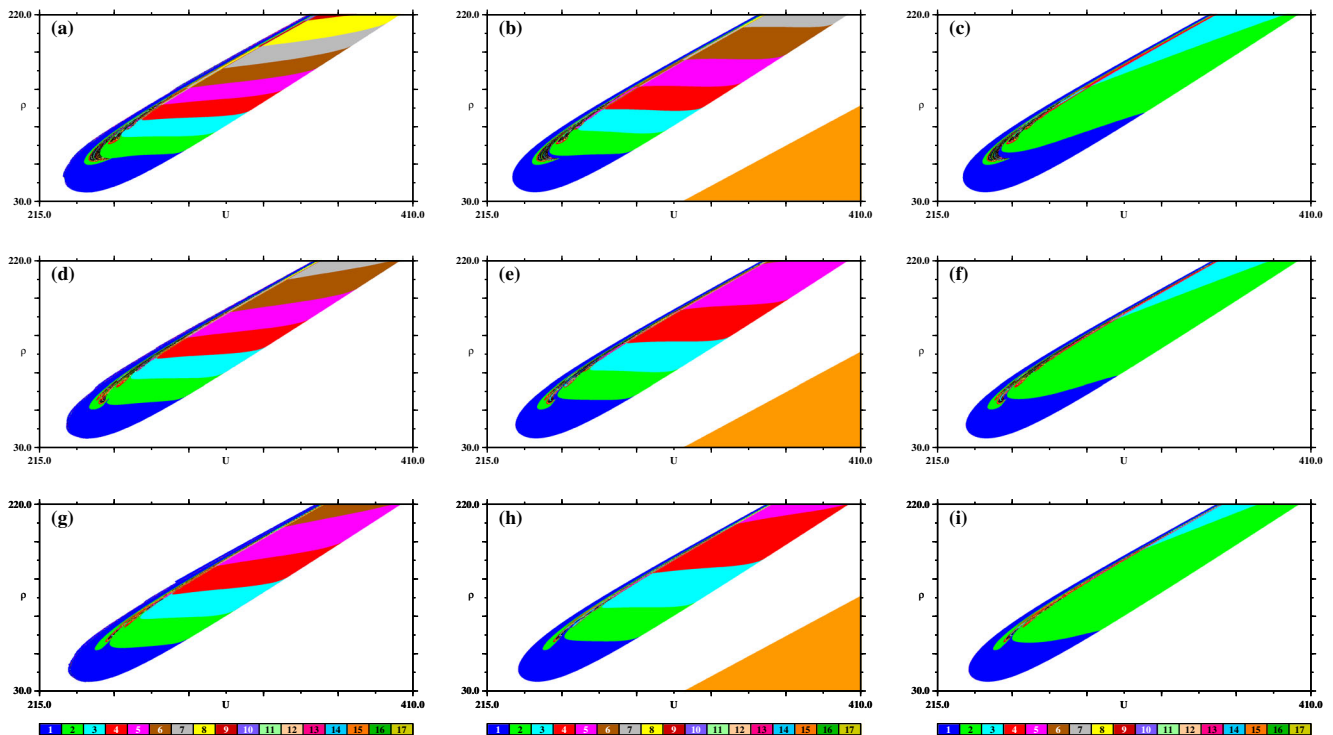


Fig. 6 Impact of the parameter ε on the number of spikes observed in the three variables φ , θ , c . Top row: $\varepsilon = 0.008$. Middle row: $\varepsilon = 0.010$. Bottom row: $\varepsilon = 0.012$. Note strong differences with respect to the cases $\varepsilon = 0.001$ (Fig. 3) and $\varepsilon = 0.005$ (Fig. 5). Legend and colors are as in Fig. 3

sequence of ten points along the line $\rho = -247.65 + 1.25 U$. The coordinates (U, ρ) of these points and the respective period of the oscillations are listed in Table 1. On the right panel, one sees a series of periodic temporal evolutions obtained for these ten representative points. The periods contain one large spike L followed by a regularly increasing number S of small oscillations, forming a sequence of mixed-mode oscillations that is usually referred to as a L^S pattern [8].

It is noteworthy in Fig. 5 that the amplitude of the smaller spikes decreases steadily, a signature of possible homoclinic behavior in the system, a behavior which can be associated with motions in two different manifolds, called slow-fast manifolds. It is important to note that this behavior can be observed in electrochemical systems and has been reported in several papers in the literature [7, 51]. In fact, it is very interesting to relate the presence of codimension-two and hubs phenomena with the existence of homoclinic behavior in the generic model since homoclinic behavior is known to be present in experimental electrochemical systems.

What is the effect of further increasing the value of ε in the control parameter space of the oscillator? The answer is given in Fig. 6, which illustrates isospike diagrams for $\varepsilon = 0.008, 0.010, \text{ and } 0.012$. As the figure shows, the system continues to predominantly show periodic oscillations despite the fact that the chaotic phases slightly increase. The net effect of increasing ε is to broaden the isospike stripes. The nonchaos-mediated mixed-mode character of the control space is preserved. The variable c , the concentration of electroactive species, is much less affected than φ , the double-layer potential, and θ , the surface coverage that blocks the faradaic reaction. An interesting open problem is to study the changes in the distribution of periodic phase located inside the chaotic phases.

Conclusions

The recent literature concerning phase diagrams computed for dissipative flows has evidenced the relative abundance and the universality of self-organized structures similar to the ones reported here. Experimental corroboration was also reported, based on measurements done in electronic circuits [14, 15]. However, in chemical systems, these phenomena have not yet been neither predicted nor observed. The importance of electrochemical systems as suitable systems to observe novel and subtle dynamics was discussed recently [19–21]. In this paper, we show that for suitably chosen control parameters, electrochemical systems are capable of displaying intricate hubs and their associated spiral dynamics.

In particular, the parameter ε accounts for the time-scale of the changes in the double-layer potential and is proportional to the electrode capacitance. The capacitance can be varied to a considerably extent by changing the electrode roughness, for instance. The first trend that emerges from the present analysis is the observed confinement of the chaotic region for increasing ε , as illustrated by Figs. 3, 5, and 6. In contrast to structures such as shrimps and spirals that might occur in very small parameter regions, the confinement of chaotic domains that would follow the increasing in the electrode capacitance seems to occur in a quite wide parameter region. This aspect definitively opens interesting perspectives for the search of a genuine codimension-two experimental equivalent of the numerically anticipated phenomena in stability diagrams reported here.

In conclusion, we have investigated the dynamics of a generic electrochemical oscillator in terms of numerically obtained Lyapunov and isospike period diagrams. Our diagrams reveal rich dynamical behaviors, including formation of spirals and hubs. The observation of mixed-mode oscillation in time series indicate the presence of nonchaos-mediated mixed-mode oscillations. In contrast with the enzyme reaction of [8], described by 10 dynamical variables and 14 parameters, the electrochemical oscillator studied here is described by just 3 variables and relatively few parameters, greatly simplifying analytical and experimental work. Despite its simplicity, it is remarkable that the three-variables electrochemical oscillator is able to capture most of the complex structures found in more complex fluxes. In the search of experimental equivalents, we are currently exploring the organization of periodic and chaotic regimes in different parameter spaces, under both potentiostatic and galvanostatic regimes.

Acknowledgments M.A.N. (Grants 2011/10982-0 and 2012/24368-4) and H.V. (Grants 2012/24152-1 and 2013/16930-7) acknowledge São Paulo Research Foundation (FAPESP) for financial support. H.V. (Grant 304458/2013-9) acknowledges Conselho Nacional de Desenvolvimento Científico e Tecnológico (CNPq) for financial support. This work was supported by the Max-Planck Institute for the Physics of Complex Systems, Dresden, in the framework of the Advanced Study Group on Optical Rare Events, and by the Deutsche Forschungsgemeinschaft through the Cluster of Excellence *Engineering of Advanced Materials*. JACG was also supported by CNPq, Brazil. All computations were done in the CESUP-UFRGS clusters in Porto Alegre, Brazil.

References

1. Strogatz S (2015) *Nonlinear dynamics and chaos with applications to physics, biology, chemistry, and engineering*, 2nd edn. Westview Press, Boulder

2. Argyris J, Faust G, Haase M, Friedrich R (2015) *An Exploration of Chaos*. Springer, New York
3. Orlik M (2012) *Self-Organization in electrochemical systems I: general principles of self-organization*. Temporal Instabilities. Springer, Berlin
4. Goldbeter A (1997) *Biochemical oscillations and cellular rhythms*. Cambridge University Press, Cambridge
5. Field RJ, Gyorgy L (1993) *Chaos in chemistry and biochemistry*. World Scientific, Singapore
6. Scott SK (1991) *Chemical chaos*. Oxford University Press, Oxford
7. Bi W, Hu Y, Cabral MF, Varela H, Yang J, Jiang R, Gao Q (2014) Oscillatory electro-oxidation of thiosulfate on gold. *Electrochim Acta* 133:308–315
8. Hauser MJB, Gallas JAC (2014) Nonchaos-mediated mixed-mode oscillations in an enzyme reaction system. *J Phys Chem Lett* 5:4187–4193
9. Junges L, Gallas JAC (2012) Frequency and peak discontinuities in self-pulsations of a CO₂ laser with feedback. *Opt Commun* 285:4500–4506
10. Gallas MR, Gallas MR, Gallas JAC (2014) Distribution of chaos and periodic spikes in a three-cell population model of cancer. *Eur Phys J Special Topics* 223:2131–2144
11. Golomb D (2014) Mechanism and function of mixed-mode oscillations in Vibrissa motoneurons. *PLoS One* 9:e109205
12. Hoff A, da Silva DT, Manchein C, Albuquerque HA (2014) Bifurcation structures and transient chaos in a four-dimensional Chua model. *Phys Lett A* 378:171–177
13. Freire JG, Cabeza C, Marti AC, Pöschel T, Gallas JAC (2014) Self-organization of antiperiodic oscillations. *Eur Phys J Special Topics* 223:2857–2867
14. Sack A, Freire JG, Lindberg E, Pöschel T, Gallas JAC (2013) Discontinuous spirals of stable periodic oscillations. *Nature Sci Rep* 3:03350
15. Freire JG, Cabeza C, Marti AC, Pöschel T, Gallas JAC (2013) Antiperiodic oscillations. *Nature Sci Rep* 3:01958
16. Francke RE, Pöschel T, Gallas JAC (2013) Zig-zag networks of self-excited periodic oscillations in a tunnel diode and a fiber-ring laser. *Phys Rev E* 87:042907
17. Manchein C, Celestino A, Beims MW (2013) Temperature resistant optimal ratchet transport. *Phys Rev Lett* 110:114102
18. Celestino A, Manchein C, Albuquerque HA, Beims MW (2011) Ratchet transport and periodic structures in parameter space. *Phys Rev Lett* 106:234101
19. Nascimento MA, Gallas JAC, Varela H (2011) Self-organized distribution of periodicity and chaos in an electrochemical oscillator. *Phys Chem Chem Phys* 13:441–446
20. Nascimento MA, Nagao R, Eiswirth M, Varela H (2014) Coupled slow and fast surface dynamics in an electrocatalytic oscillator: model and simulations. *J Chem Phys* 141:234701
21. Vitolo R, Glendinning R, Gallas JAC (2011) Global structure of periodicity hubs in Lyapunov phase diagrams of dissipative flows. *Phys Rev E* 84:016216
22. Barrio R, Blesa F, Serrano S, Shilnikov A (2011) Global organization of spiral structures in biparameter space of dissipative systems with Shilnikov saddle-foci. *Phys Rev E* 84:035201
23. Barrio R, Blesa F, Serrano S (2012) Topological changes in periodicity hubs of dissipative systems. *Phys Rev Lett* 108:214102
24. Sparrow C, Glendinning P (1984) Local and global behavior near homoclinic orbits. *J Stat Phys* 35:645–696
25. Gaspard P, Kapral R, Nicolis G (1984) Bifurcation phenomena near homoclinic systems: a two-parameter analysis. *J Stat Phys* 35:697–727
26. Freire JG, Gallas JAC (2010) Non-Shilnikov cascades of spikes and hubs in a semiconductor laser with optoelectronic feedback. *Phys Rev E* 82:037202
27. Gallas JAC (2010) The structure of infinite periodic and chaotic hub cascades in phase diagrams of simple autonomous systems. *Int J Bifurc Chaos* 20:197–211
28. Freire JG, Field RJ, Gallas JAC (2009) Relative abundance and structure of chaotic behavior: the nonpolynomial Belousov–Zhabotinsky reaction kinetics. *J Chem Phys* 131:044105
29. Bonatto C, Gallas JAC (2008) Periodicity hub and nested spirals in the phase diagram of a simple resistive circuit. *Phys Rev Lett* 101:054101
30. Pugliese E, Meucci R, Euzzor S, Freire JG, Gallas JAC (2015) Complex dynamics of a dc glow discharge tube: experimental modeling and stability diagrams. *Nature Sci Rep* 5:08447
31. Varela H, Krischer K (2001) Nonlinear phenomena during electrochemical oxidation of hydrogen on platinum electrodes. *Catal Today* 70:411
32. Krischer K, Varela H (2003) Oscillations and other dynamic instabilities. In: Vielstich W, Lamm A, Gasteiger HA (eds) *Handbook of fuel cells: fundamentals technology, applications*, vol 2. Wiley, Chichester, p 679
33. Nagao R, Epstein IR, Gonzalez ER, Varela H (2008) Temperature (over)compensation in an oscillatory surface reaction. *J Phys Chem A* 112:4617–4624
34. Boscheto E, Batista BC, Lima RB, Varela H (2009) A surface-enhanced infrared absorption spectroscopic (SEIRAS) study of the oscillatory electro-oxidation of methanol on platinum. *J Electroanal Chem* 642:17
35. Sitta E, Nascimento MA, Varela H (2010) Complex kinetics, high frequency oscillations and temperature compensation in the electro-oxidation of ethylene glycol on platinum. *Phys Chem Chem Phys* 12:15195
36. Martins AL, Batista BC, Sitta E, Varela H (2008) Oscillatory instabilities during the electrocatalytic oxidation of methanol on platinum. *J Braz Chem Soc* 19:679–687
37. Angelucci AC, Varela H, Herrero E, Feliu JM (2009) Activation energies of the electrooxidation of formic acid on Pt(100). *J Phys Chem C* 113:18835–18841
38. Nagao R, Cantane DA, Lima FHB, Varela H (2012) The dual pathway in action: decoupling parallel routes for CO₂ production during the oscillatory electro-oxidation of metanol. *Phys Chem Chem Phys* 14:8294–8298
39. Varela H (2012) Spatiotemporal pattern formation during electrochemical oxidation of hydrogen on platinum. *ChemistryOpen* 1:165–168
40. Krischer K (1999) *Principles of spatial and temporal pattern formation in electrochemical systems*. In: Conway BE, Bockris J, White R (eds) *Modern aspects of electrochemistry*. Kluwer, New York, p 1
41. Koper MTM, Sluyters JH (1994) Electrochemical oscillators: their description through a mathematical model. *J Electroanal Chem* 303:7394
42. Koper MTM, Sluyters JH (1994) Instabilities and oscillations in simple models of electrocatalytic surface reactions. *J Electroanal Chem* 371:149159
43. Strasser P, Eiswirth M, Koper MTM (1999) Mechanistic classification of electrochemical oscillators—an operational experimental strategy. *J Electroanal Chem* 478:50
44. Koper MTM (1996) Oscillations and complex dynamical bifurcations in electrochemical systems. In: Prigogine I, Rice SA (eds) *Advances in chemical physics*. Wiley, New York, p 161
45. Freire JG, Gallas JAC (2011) Stern-Brocot trees in cascades of mixed-mode oscillations and canards in the extended Bonhoeffer–van der Pol and the FitzHugh–Nagumo models of excitable systems. *Phys Lett A* 375:1097–1103

46. Freire JG, Gallas JAC (2011) Stern-Brocot trees in the periodicity of mixed-mode oscillations. *Phys Chem Chem Phys* 13:12191–12198
47. Freire JG, Pöschel T, Gallas JAC (2012) Stern-Brocot trees in spiking and bursting of sigmoidal maps. *Europhys Lett* 100:48002
48. Marszalek W (2012) Circuits with oscillatory hierarchical Farey sequences and fractal properties. *Circ Syst Signal Process* 31:1279–1296
49. Podhaisky H, Marszalek W (2012) Bifurcations and synchronization of singularly perturbed oscillators: an application case study. *Nonlin Dyn* 69:949–959
50. Marszalek W, Trzaska Z (2014) Mixed-mode oscillations and chaotic solutions of jerk (Newtonian) equations. *J Comp Appl Math* 262:373–383
51. Oliveira CP, Lussari NV, Sitta E, Varela H (2012) Oscillatory electro-oxidation of glycerol on platinum. *Electrochim Acta* 85:674–679